*metals*

MDPI

*Article*

# Influences of Second Phase Particle Precipitation, Coarsening, Growth or Dissolution on the Pinning Effects during Grain Coarsening Processes

**Zhiqiang Li [1,*], Shengyang Zhang [2], Yang He [1], Fei Peng [1] and Yude Liu [1]**

[1] School of Artificial Intelligence, Beijing Technology and Business University, Beijing 100048, China
[2] Institute for Advanced Materials and Technology, University of Science and Technology Beijing, Beijing 100083, China
* Correspondence: zhql041989@126.com

**Abstract:** A cellular automata model was established to simulate grain coarsening processes pinned by second-phase particles. The influences of particle coarsening, precipitation, growth and dissolution, which contain complex changes of size and number density of the particles, on the grain coarsening kinetics were investigated by considering the following two factors: average pinning force per particle and particle number density. The simulation results showed that the average pinning force per particle was related to the particle size, but little influenced by the particle number density. The investigations about the grain boundary/particles interactions showed that the increase of number fraction of particles, which located at the grain boundary junctions, should be the reason for the increase of average pinning force per particle. Then the limiting grain size was researched and compared to the results of some other models. The results showed that the average number of particles to stagnate a grain was related to both the number density and size of particles. At last, the comparisons between the present simulation results and the other simulation and experimental results showed that the present models were efficient in simulating the grain coarsening processes pinned by second-phase particles.

**Keywords:** cellular automata model; second-phase particle; grain boundary/particles interaction; grain coarsening

check for updates

**Citation:** Li, Z.; Zhang, S.; He, Y.; Peng, F.; Liu, Y. Influences of Second Phase Particle Precipitation, Coarsening, Growth or Dissolution on the Pinning Effects during Grain Coarsening Processes. *Metals* **2023**, *13*, 281. https://doi.org/10.3390/met13020281

Academic Editors: Angelo Fernando Padilha, Eric Hug and Joan-Josep Suñol

Received: 7 November 2022
Revised: 21 December 2022
Accepted: 19 January 2023
Published: 31 January 2023

**Copyright:** © 2023 by the authors. Licensee MDPI, Basel, Switzerland. This article is an open access article distributed under the terms and conditions of the Creative Commons Attribution (CC BY) license (https://creativecommons.org/licenses/by/4.0/).

## 1. Introduction

Grain refinement is an important means to improve strength and toughness of metallic materials. The second phase particles always lead to fine grains by restricting the movement of grain boundary during the processing and service of metallic materials [1–3]. Therefore, the particle pinning effects during the grain coarsening processes always received extensive attentions.

Though there were many experimental researches on the grain coarsening processes pinned by second phase particles, many variables were difficult to control and measure accurately and the conclusions were difficult to be extended to other materials in these researches. Therefore, the mathematical models were widely used to deal with more general situations. As the status of second phase particles and the grain boundary/particles interactions were complicated, analytic expressions for the grain coarsening kinetics pinned by second phase particles were very difficult to be obtained. Therefore, many computational simulation models, including the Monte-Carlo (MC) [4–13], front-tracking (or vertex) [14–17], phase-field (PF) [18–29], finite element [30–32] models and so on, were used. The influences of the particle shapes, such as circular, elliptical in 2 dimensions [22] and rod like [24], spherical [25], ellipsoidal [27], cubic [25,27] in 3 dimensions, were researched with PF models in detail. Reference [22] researched the influences of particle size and shape on the grain coarsening kinetics, respectively. They also showed that pinning force was independent of grain size

in 2 dimensions by simulating the interactions between a single particle and single grain boundary. Reference [24] researched the influences of orientation and length/diameter ratio of rod like particles on the grain coarsening kinetics. Reference [25] researched the effects of size distribution and morphology on grain coarsening kinetics. Reference [27] researched relationships between the shape and pinning force for spherical and ellipsoidal particles. The influences of the distributions [16], mobility [26] and coherency [28] of the particles were also investigated. Reference [16] researched the influences of pinning strength and spatial distribution on the grain coarsening kinetics with a vertex model. Reference [26] researched the interactions between mobile particles and grain boundary with one- and two-dimensional PF models during grain coarsening processes. Reference [28] researched the influences of particle/matrix coherency on the grain coarsening kinetics with a 3-dimensional PF model. The numerical models greatly promoted the investigations of the second-phase particle pinning effects on the grain boundaries. All these researches focused on the influences of the second phase particles on grain coarsening kinetics during various of single factor change processes.

However, in actual heat treatment processes, the evolutions of the particles would be more complicated. Such as during the particle coarsening processes, the number and size of the particles should be changed simultaneously, but the total volume fraction should be maintained; during the particle growth on dissolution processes, the changes of the particle size was considered to be dominant; during the particle precipitation processes, the increasing of the particle number should be focuses on, but the changes of the particle size were always ignored. Numerical simulation researches on the influences of these specific particle evolution processes on the grain coarsening kinetics were significant but lacked so far.

In the present literature, the 2-dimensional (2D) cellular automata (CA) model was established basing on our previously proposed grain boundary/particles interaction model [33]. Then the influences of particle coarsening, precipitation, growth and dissolution on the grain coarsening kinetics were investigated by considering the two factors, including average pinning force per particle and particle number density, with the model. The interactions between the grain boundary and particles were also investigated to explain the phenomena.

## 2. Models

The 2D CA model used in the present research has been introduced in our previous articles [33,34]. The moving velocity of grain boundary could be calculated with the following formula [35]:

$$V = M\sigma_{gb}\kappa \tag{1}$$

where $M$, $\sigma_{gb}$ and $\kappa$ were the mobility, energy and curvature of the grain boundary, respectively.

In the CA model, the regions of the material to be simulated were discretized to small cells. Then each cell was set state parameters to indicate the grain orientation. In each calculation step, the state of a cell was decided by its four edge contacted neighbor cells. As shown in Figure 1, the grain boundary curvature was calculated basing on the status of the cells in the curvature calculation area with our modified Mason's 2D curvature calculation model [36,37]:

$$\kappa = \exp\left(\frac{\omega^2\lambda^2}{2\eta^2}\right)\left[\frac{\lambda^2 D}{\sqrt{2\pi}\eta^3} - \frac{\sqrt{2\pi}}{\eta}erf\left(\frac{\omega\lambda}{\sqrt{2}\eta}\right)\right] \tag{2}$$

where $\omega$ = 0.5 was a constant and $\eta$ = 1.19λ. The value of $D$ could be obtained from the status of the cells in the curvature calculation area [37]. This modified 2D curvature model has been validated by comparing the results to the classical models in our previous research [37].

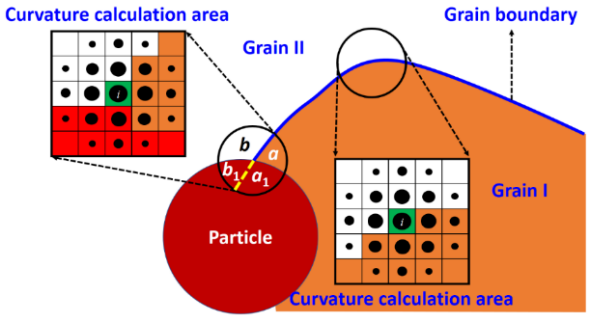



**Figure 1.** Diagrams of curvature calculation methods for the normal grain boundary and the grain boundary/particle junction.

As shown in Figure 1, at the location where the grain boundary and the particle contacted with each other, part of the grain boundary was replaced by the particle and the cell status needed to calculate the grain boundary curvature was lacked. To obtain the full information of the curvature calculation area, the lost grain boundary was completed by extending into the particle. Then the corresponding cell status in the virtual curvature calculation area in the particle could be derived from the cell status outside the virtual curvature calculation area by solving the following equations:

$$a_1 = (a_1 + b_1)\frac{b}{a+b} \tag{3}$$

$$b_1 = (a_1 + b_1)\frac{a}{a+b} \tag{4}$$

where $a$, $b$, $a_1$ and $b_1$ were the areas of the regions as shown in Figure 1. This curvature calculation model for the grain boundary/particle junction was validated by comparing the simulation results for the interactions of single particle and grain boundary to the corresponding results of the classical theories in our previous published article [34]. In this previous article, the influences of the particle/grain interfacial energy on the grain coarsening process were also researched and obtained reasonable results [34].

The frequency of the status of cell ($i$,$j$) to be transformed to the status of its neighbor cells was calculated with the following formula:

$$v_{i,j} = \sum_{(g,h)\in A(i,j)} V_{g,h}/\lambda \tag{5}$$

where $A$ ($i$,$j$) was a set containing all the two layers of neighbor cells of cell ($i$,$j$); $V_{g,h}$ was the grain boundary moving velocity of neighbor cell ($g$,$h$), has units of m·s$^{-1}$; $\lambda$ was the side length of the cells, has unit of m. During the calculation process, the maximum time steps ensuring the transformation frequency of every cell bellow 1 were used to balance calculation efficiency and accuracy.

## 3. Model Parameters and Simulation Conditions

The initial grain microstructure was obtained by a 2D CA recrystallization model, then different structures of the second phase particles were generated in the same initial grain microstructure. The average grain radius of the initial grain microstructure was 22 μm. The grain coarsening processes were simulated in domains with 800 × 800 cells, which were proven to be appreciate in our previous research [36]. The length of the cell side was 1.3 μm. The grain boundary energy and mobility were set to be $\sigma_{gb}$ = 0.56 J·m$^{-2}$ [38] and $M$ = 3.4 × 10$^{-11}$ m·s$^{-1}$Pa$^{-1}$ [39], respectively, for fcc Fe.

## 4. Results and Discussion

### *4.1. The Grain Coarsening Kinetics*

Figure 2 showed the calculation results of the microstructures and average grain sizes, which evolved from the same initial grain structures randomly dispersed with second phase particles of different radii and area fractions. As shown in Figure 2a, the simulation conditions A and C had the same particle area fraction of $f_V$ = 0.08, but different particle radii of $r$ = 3.9 and 7.8 μm, respectively. The changes of the simulation conditions from A to C were corresponding to a particle coarsening process. The simulation conditions B and C had the same particle number of $N$ = 445. The changes of the simulation conditions from B to C should be corresponding to a particle growth process. Note that the growth process here was the process that the particle size growing but the particle number remained constant. It was different to the coarsening process, during which the area fraction of particles remained constant. From the simulation conditions of B to A, the number density of the particles increased, these changes were corresponding to a particle precipitation process. Figure 2a showed the simulation results of the stagnating microstructures for different simulation conditions. The simulation results obviously showed that the coarsening and dissolution of particles could both weaken the pinning effects, and the growth and precipitation increased the pinning effects.

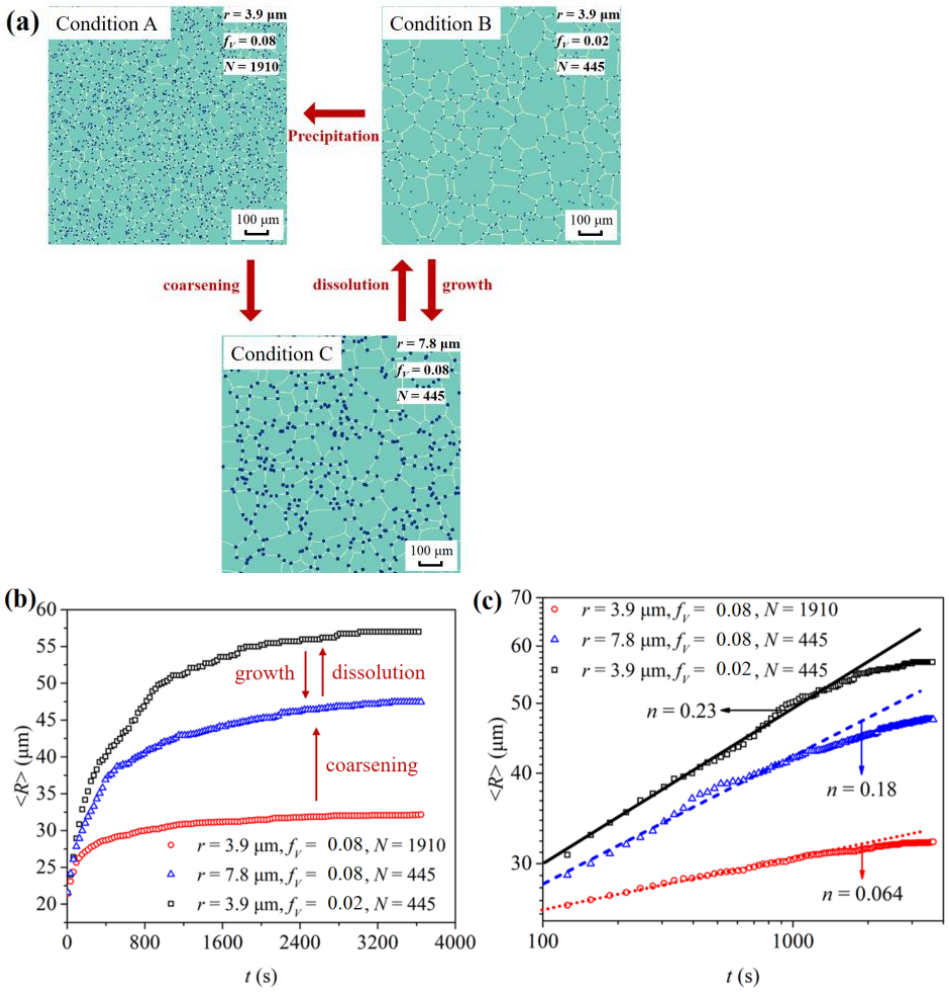



**Figure 2.** Simulation conditions and simulation results of the grain coarsening kinetics. (**a**) Simulation conditions and the corresponding stagnating microstructures. (**b**) Relationships between the grain radii and coarsening time for different conditions. (**c**) Logarithmic relationships between the grain radii and coarsening time.

Figure 2b showed the simulated average radii of the grains for different simulation conditions. The grain coarsening kinetics pinned by randomly distributed second-phase particles was always expressed by the following power formula:

$$< R >= kt^n \tag{6}$$

where $k$ was the material parameter; $n$ was the index of grain growth. Figure 2c showed the logarithmic scale of Figure 2b. As shown in Figure 2c, the linear relationships between logarithmic grain radius and time described by Equation (6) were only observed during the initial stages of rapid growth. This simple relationship for the grain coarsening kinetics was originated from simple generalization of the exponential relationship for the normal grain coarsening process. In the initial stages of grain coarsening, the driving forces of grain coarsening were much larger than the pinning forces of the particles, the grain coarsening kinetics was close to the normal grain coarsening, thus the relationships described by Equation (6) were suitable in the initial stages. In the ending stages, the relationships between logarithmic grain radius and time deviated from the linear relationships. During these stages, the driving forces of the grain coarsening decreased with the increasing of grain size; on the other hand, more and more grain boundaries contacted with the particles during the increasing of grain size, thus leading to the increase of pinning forces. Therefore, the differences between the driving and pinning forces decreased during the grain coarsening processes. This leaded to the deviations of the relationships between logarithmic grain radius and time from the linear relationship in the ending stages.

To investigate the influences of the complex particle changes, such as the particle coarsening, precipitation, growth and dissolution, on the grain coarsening kinetics, we described the particles with two factors: the average pinning force per single particle and the particle number density. As the particle number density changes during these processes were easy to be understood and their influences on the grain coarsening kinetics were also widely investigated, the present research mainly focused on the average pinning force per single particle.

Differential form of the grain coarsening kinetics pinned by second-phase particles could be expressed by the following equation:

$$\frac{\mathrm{d} < R >}{\mathrm{d}t} = M(P_d - P_z) \tag{7}$$

where <$R$> was average grain radius, had unit of m; $t$ was coarsening time, had unit of s. $P_d$ and $P_z$ were the grain coarsening driven force and particle pinning force, respectively. As the average grain coarsening driven force was decided by the average grain boundary curvature, which could be expressed with 1/<$R$>, the difference of the pinning force between two grain coarsening processes could be written as:

$$\Delta P_z = \left[ \left( \frac{d < R >}{dt} \right)_1 - \left( \frac{d < R >}{dt} \right)_2 \right] / M \tag{8}$$

Figure 3a showed the relationships between the average grain boundary moving velocities (d<$R$>/d$t$) and the average grain radii (<$R$>) for the simulation conditions A and C. As shown in the figure, the average grain boundary moving velocity decreased with the average grain radii for the decreasing of the average grain boundary curvature. The figure also showed that the grain boundary moving velocities obviously increased after the second-phase particles were coarsened from $r$ = 3.9 μm to $r$ = 7.8 μm. Substituting the data shown in Figure 3a into Equation (8), the differences of the pinning force between simulation conditions A and C were obtained and shown in Figure 3b. As shown in Figure 3b, the differences of pinning force didn't change much during the grain coarsening processes. The average value of $\Delta P_z$ was calculated to be 905.1 J·m$^{-3}$.

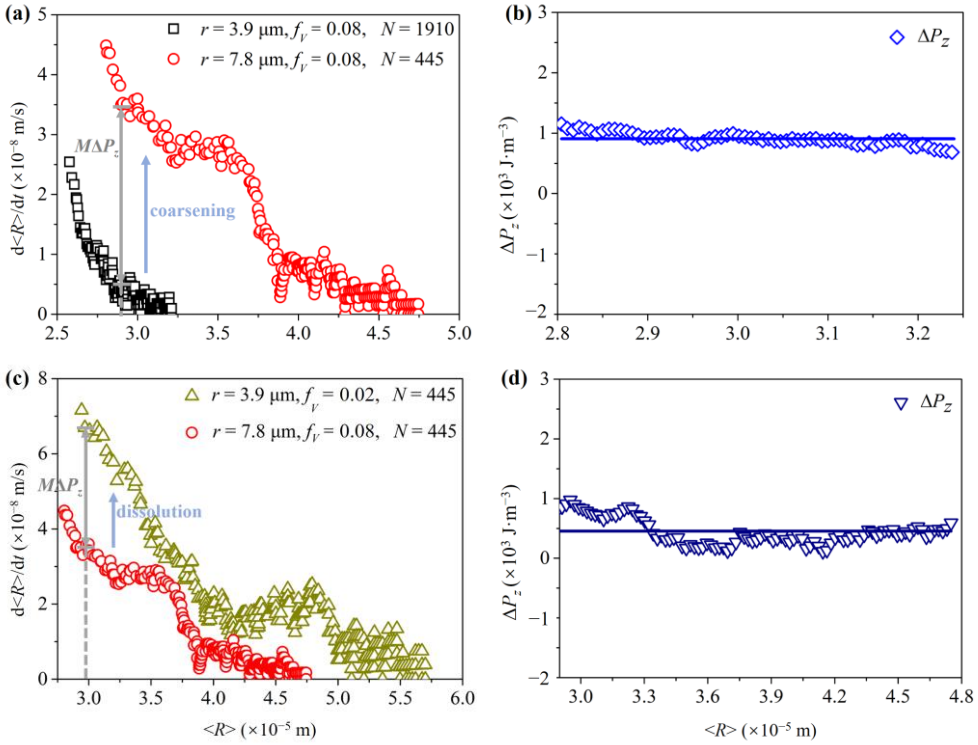



**Figure 3.** Calculation results for the grain boundary moving velocities and pinning force differences of the particles. Differences of grain boundary moving velocity between (**a**) simulation conditions A and C and (**c**) simulation conditions B and C. Differences of the pinning force between (**b**) simulation conditions A and C and (**d**) simulation conditions B and C.

Figure 3c showed the relationships between the grain boundary moving velocity and the average grain radius for the simulation conditions B and C. The figure showed that the grain boundary moving velocity increased when the particle radius decreased from $r$ = 7.8 μm to $r$ = 3.9 μm. The differences of the pinning force between simulation conditions B and C were also calculated from the data of Figure 3c and then shown in Figure 3d. As shown in Figure 3d, the values of $\Delta P_z$ decreased rapidly at the beginning of the coarsening process, then did not change much in the steady coarsening stage. This was induced by the unsteady grain boundary/particles interactions in the beginning stage and would be shown in Section 4.3. The average value of $\Delta P_z$ was calculated to be 494.9 J·m$^{-3}$.

According to the research of Hillert [40], the particle pinning force for 2D grain coarsening was calculated with the following formula:

$$P_z = z\frac{\sigma_{gb} f_V}{r} \tag{9}$$

where $z$ was the Zener factor; $f_V$ was the particle area fraction. Then $\Delta P_z$ was expressed with the following formula:

$$\Delta P_z = z\sigma_{gb}\left(\frac{f_{V1}}{r_1} - \frac{f_{V2}}{r_2}\right) \tag{10}$$

The subscripts 1 and 2 indicated different conditions of the second phase particles. Substituting the average values of $\Delta P_z$ obtained from the simulation data, the values of $z$ were calculated to be 0.19 and 0.2 for the particle coarsening and dissolution situations, respectively. For the particle precipitation situation as shown in Figure 2a, the value of $\Delta P_z$ should be equal to the sum of these values for the particle coarsening and dissolution situations. Then the value of $z$ for the particle precipitation situation was calculated to be 0.19. As the values of $z$ for the particle coarsening, dissolution/growth and precipitation

situations were very close to each other, the relationships between the pinning force and particle fraction and size as shown in Equation (9) were still valid in the present model. Though the values of $z$ obtained with the present model were much smaller than the value of $4/\pi$ for Zener's 2D model, the average value of $z$ could be used to calculate the values of $P_z$. The calculation results of the pinning forces for the simulation conditions A, B and C were 1904, 476 and 952 J·m$^{-3}$. According to Zener's model, the pinning force could be expressed as [41],

$$P_z = N_b F_z \tag{11}$$

where $N_b$ was the number of particles in contact with the grain boundary per unit area. $F_z$ was the average pinning force per particle. Figure 4 showed the number fractions of the particles contacting with the grain boundary ($\varphi$) for different simulation conditions. As shown in the figure, the fractions of grain boundary particles increased rapidly in the beginning stages and then maintained almost stable. The values of $N_b$ could be calculated with the following formula:

$$N_b = \frac{N\varphi_{as}}{S_c} \tag{12}$$

where $\varphi_{as}$ was the average grain boundary particle fraction in the stable stage. $S_c$ was the area of the simulation region. $N$ was the total number of the particles. Substituting Equation (12) to Equation (11), the values of $F_z$ for the simulation conditions A, B and C were calculated to be $1.32 \times 10^{-6}$, $1.36 \times 10^{-6}$ and $2.43 \times 10^{-6}$ J·m$^{-1}$, respectively. The values of $F_z$ for conditions A and B, which both had particle radius of 3.9 μm, were very close to each other, but much lower than the $F_z$ value for condition C, which had a particle radius of 7.8 μm. These results meant that the average pinning force per particle relied heavily on the particle size, but little influenced by the particle number density. These results seem to different from the previous theory about the 2D systems, which showed that the pinning force of a 2D particle was independent of the particle size ($F_z = 2\sigma_{gb}$) [15,40]. To further understand these mechanisms, the interactions between the particles and the grain boundary should be explored.

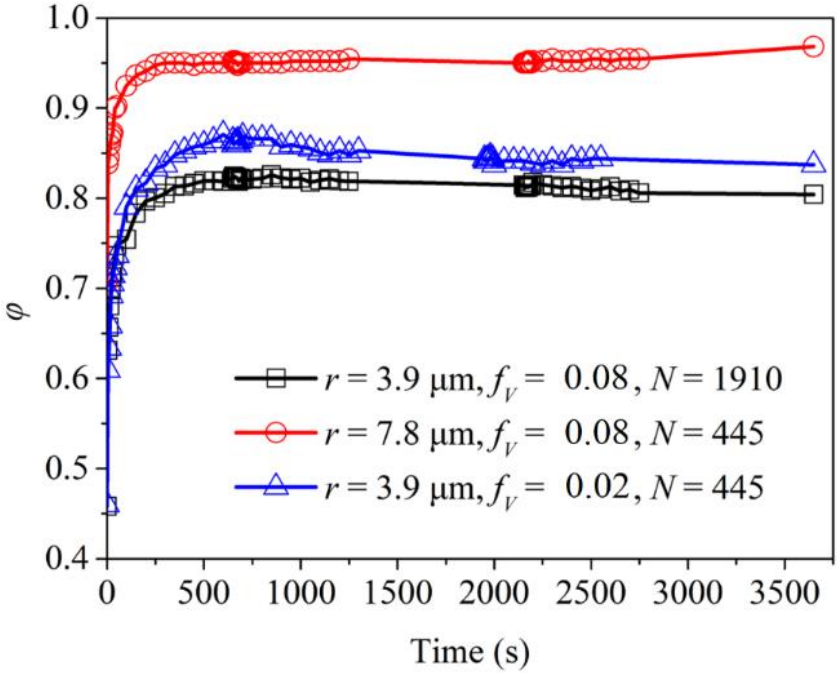



**Figure 4.** Evolutions of the number fractions of the particles contacting with grain boundary.

### *4.2. The Grain Boundary/Particles Interations*

Figure 5a–c showed the number fractions of particles, which were located at the grain boundaries or junctions. As shown in the figures, the total number fractions of the particles, which were located at the grain boundary and junctions (TFPLBJ), rapidly increased first and gradually reached the limiting values in the latter processes. As shown in Figure 5a,b, the TFPLBJ decreased slightly after achieved the limiting values. This meant that the simulation results for $r$ = 3.9 μm showed grain boundary de-pinning actions. As the decreasing tendency of the TFPLBJ in Figure 5b was larger than in Figure 5a, the decrease of particle number should increase the de-pinning actions. According to Section 4.1, as the average pinning force per particle for Figure 5b was even a little more than that for Figure 5a, the average pinning force per particle was not the reason for the increase of de-pinning actions from Figure 5a to Figure 5b. Therefore, the increase of the grain coarsening driving force should be the reason for the increase of the de-pinning actions. As the de-pinning of the particles was not found in Figure 5c, the comparison between Figure 5b,c would show that the de-pinning actions was also reduced when only the particle radius increased. According to Section 4.1, the average pinning force per particle for Figure 5c was much larger than that for Figure 5a,b, thus the decrease of the de-pinning actions should be also induced by the increase of the average pinning force per particle. Synthesizing the two comparative analysis results, the de-pinning actions of the particles relied on both the driving and pinning force and influenced by both the particle size and number density. The theory that the pinch off actions of particles was independent of particle size, which was originally proposed by Hillert basing on that the pinning force was independent of particle size in 2D [40], should be modified.

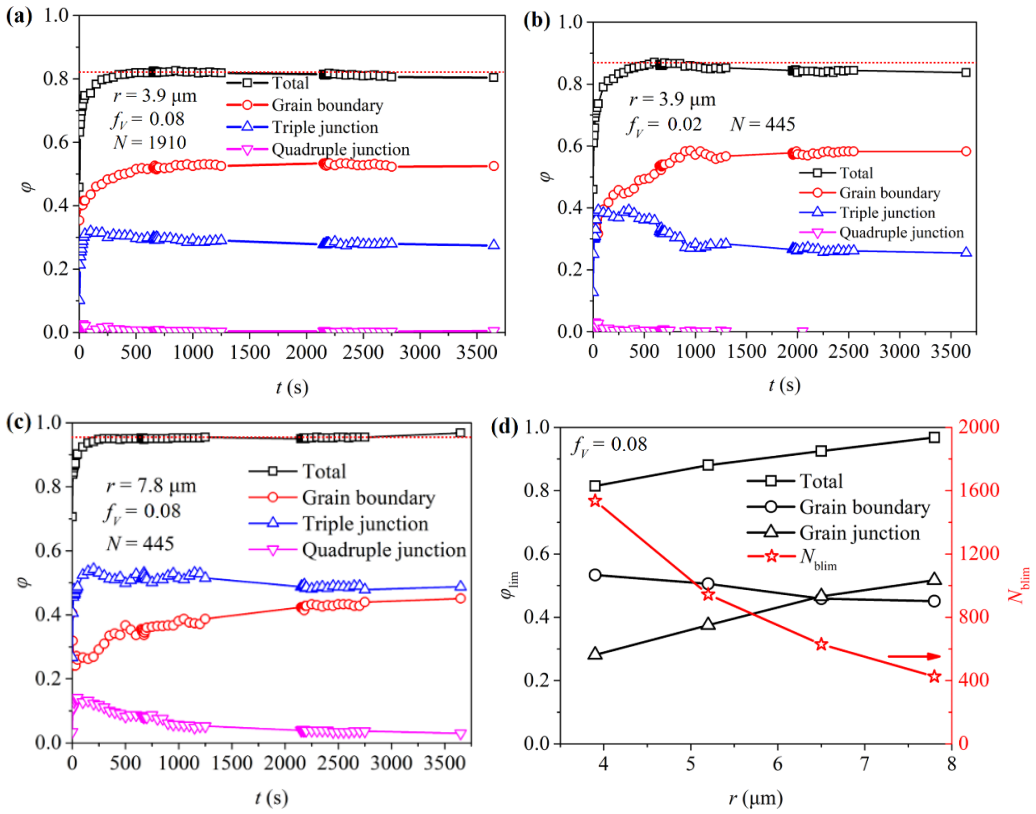



**Figure 5.** Evolutions of the particle locations during the grain coarsening processes for different simulation conditions. (**a**) $r$ = 3.9 μm, $f_V$ = 0.08; (**b**) $r$ = 3.9 μm, $f_V$ = 0.02; (**c**) $r$ = 7.8 μm, $f_V$ = 0.08; (**d**) The changes of the limiting number fraction ($\varphi_{lim}$) and the absolute number ($N_{blim}$) of the particles for different particle radii but the same particle area fraction of $f_V$ = 0.08.

The previous researches showed that the particle size should have little influences on the pinning force when a single grain boundary was pinned by a single particle in the 2D system [15,40]. However, in an actual system, a particle could in contact with more than 1 grain boundary and changed the relative position continuously. Figure 6 showed the simulated microstructures for $r$ = 7.8 μm and $f_V$ = 0.08 when $t$ = 100 and 350 s. The red-arrow-marked 3 particles in the microstructure were all in contact with the grain quadruple junctions when $t$ = 100 s. As the grains continued to coarsen, 2 of the particles were in contact with grain triple junctions and the other one was in contact with the grain boundary when $t$ = 350 s. The evolution of the microstructure showed that the grain quadruple junctions tended to transfer to triple junctions or grain boundaries for their unstable structures. As shown in Figure 6, there should be different pinning forces of the particles with different locations. When the particle was located at the grain boundary, it would pin only 1 grain boundary; however, when the particle was located at a triple or quadruple junction, it would pin more grain boundaries. Table 1 showed the limiting number fractions of particles at different locations for the simulation conditions A, B, and C. As shown in the table, the limiting number fractions for conditions A and B were close to each other, however, the limiting number fractions of particles in contact with grain junctions for condition C was much larger than that for condition A and B. This should be the reason for the average pinning force per particle for condition C was much larger than that for condition A and B.

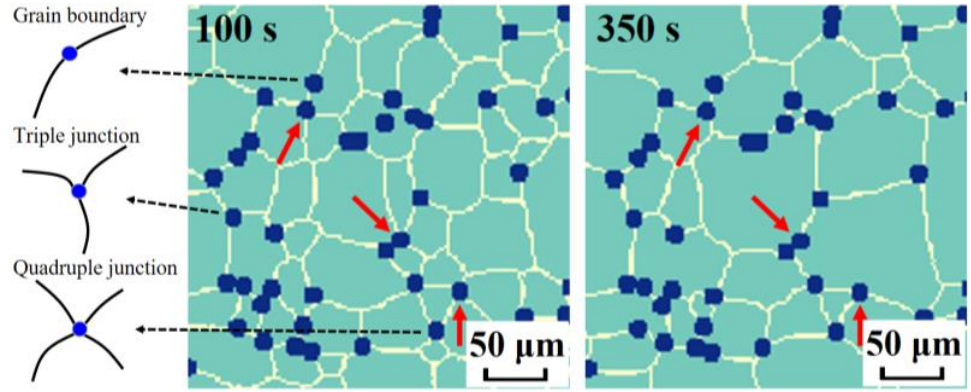



**Figure 6.** Simulated microstructures for $r$ = 7.8 μm and $f_V$ = 0.08 when $t$ = 100 and 350 s.

**Table 1.** Limiting number fractions of particles contacting with grain boundary, triple junction and quadruple junction for different simulation conditions.

| Limiting Number Fraction \ Simulation Condition | A | B | C |
|---|---|---|---|
| Boundary | 0.53 | 0.58 | 0.43 |
| Triple junction | 0.28 | 0.26 | 0.49 |
| Quadruple junction | 0.0033 | 0.0022 | 0.037 |

Figure 5d showed the changes of the limiting number fractions ($\varphi_{lim}$) and the absolute numbers ($N_{blim}$) of the particles, which were located at grain boundary or junctions, for different particle radii but the same particle area fraction of $f_V$ = 0.08. Under these simulation conditions, the particle radius changed but the particle area fraction was maintained. This should be corresponding to the particle coarsening process. According to the figure, there should be two elements that changed the particle pinning force. One was the particle locations: the increase of the number fraction of junction particles will lead to an increase tendency of the pinning force, as analyzed above. The other one was the absolute number of particles: the decrease of the particle absolute number would lead to a decrease tendency of the pinning force. Overall, the decrease of the pinning effects during the particle coarsening

process should be the results of the competition between the effects of particle locations (at grain boundary or junctions) and $N_{blim}$.

The researches of Darling et al. [41–43] showed that the coarsening of oxide particles will lead to the increase of grain size and decrease of the yield strength of Fe-Ni-Zr oxide-dispersion strengthened (ODS) alloys. On the other hand, they also found that the smaller grain sizes and particles appear to be more sensitive to thermal softening than larger grains and larger particles. Achieving and retaining high strengths above 600 °C, the size of the particle should be not too small or too large. According to the present research, considering both the influences of the particle size and number density on the pinning force should be necessary, especially when the quantitative evaluations of the pinning force was needed, during maximize the tradeoffs between the particle sizes for ODS alloys.

The abnormal grain growth always occurred when the pinning force of the particles decreased during the grain coarsening processes [44], such as the grain coarsening was accompanied by the particle dissolution or coarsening, or the distribution of the particles was non-random. However, the particles in the present model were set to be stable and the distributions were random. Thus, the abnormal grain growth was not occurred in the present simulations. According to the present research, the changes of the pinning force induced by the particle size increase or decrease should be considered during the investigation of the abnormal grain growth phenomenon in 2 dimensions.

### *4.3. The Stagnating Average Grain Size*

According to the classical Zenner's pinning theory [45], the stagnating average grain size of a second-phase particles pinned structure could be calculated with the following formula:

$$\frac{< R >_{\lim}}{r} = \beta \frac{1}{f_V^{\xi}} \tag{13}$$

where $\beta$ and $\xi$ were two constants, respectively equal to 4/3 and 1. $<R_{lim}>$ was the stagnating average grain radius. In fact, not all of the particles were located at the grain boundaries or junctions, so the factor $f_V$ in equation (13) was always modified with $\varphi_{\lim}$ [45]:

$$\frac{< R >_{\lim}}{r} = \beta \frac{1}{(\varphi_{\lim} f_V)^{\xi}} \tag{14}$$

As shown in Figure 7a, the linear relationships for different particle radii showed that the simulation results of the present model were in accordance with the Zenner's and the modified Zenner's pinning theories, as shown in Equations (13) and (14), respectively. The figure also showed various slopes for different particle radii. Figure 7b shows the simulated values of $\xi$ and $\beta$ for different particle radii. As shown in the figure, the values of $\xi$ increased with the particle radius. For the simulated largest radius of $r$ = 7.8 μm, the values of $\xi$ were close to 0.5, which was widely obtained with other 2D models. For other smaller particle radii, the values of $\xi$ were smaller than 0.5. The results of 2D phase field model [21] also showed some simulation results of $\xi$ (for $f = f_V$) smaller than 0.5. However, they thought that the values of $\xi$ for the modified $f = \varphi_{\lim} f_V$ should be close to 0.5. The present results showed that the values of $\xi$ for the modified $f = \varphi_{lim} f_V$ were larger than the values of $\xi$ for $f = f_V$, which tended to be in accordance with the 2D phase field simulation results, but not all close to 0.5. The figure also showed that the values of $\beta$ decreased with the particle radius. For the modified $f = \varphi_{lim} f_V$, the values of $\beta$ were a little smaller than the values for original $f = f_V$. For the simulated largest radius of $r$ = 7.8 μm, the values of $\beta$ were respectively 1.8 and 1.53 for $f = f_V$ and $f = \varphi_{lim} f_V$, which were close to the values of 1.2 to 1.8 obtained by other models [4,6,18]. For other smaller particle radii, the values of $\beta$ were larger. The 2D phase field simulation obtained a value of $\beta$ = 4.4 [21], which were close to the results of the present model for $r$ = 2.6 μm.

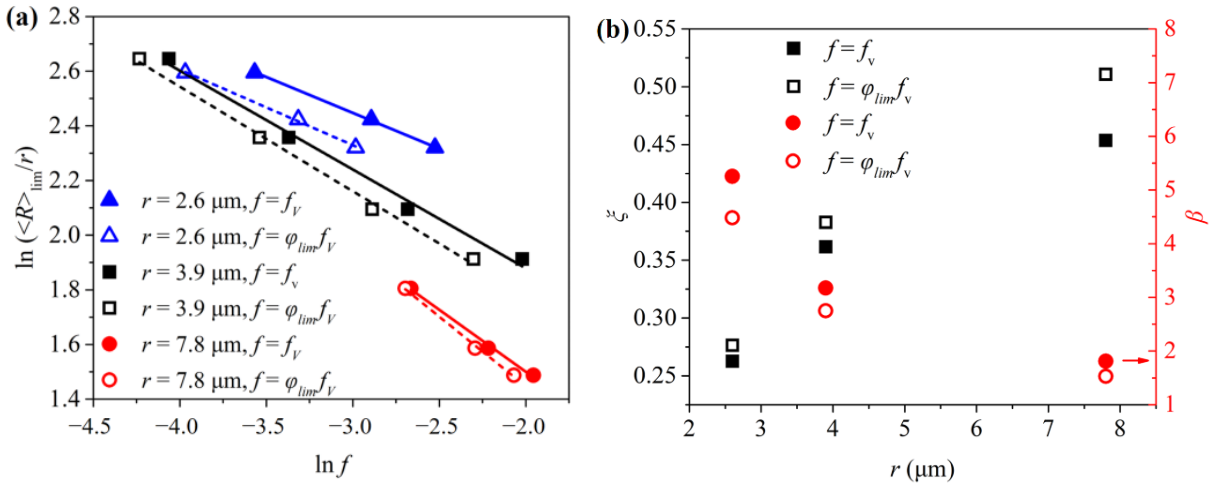



**Figure 7.** The comparisons between the present simulation results and the Zener's and the modified Zenner's pinning theories. (**a**) The fitting results for Equations (13) and (14); (**b**) values of $\xi$ and $\beta$ for different particle radii.

According to the theory of Srolovitz et al. [4], 3 particles were needed to stagnate the grains in 2D system, then the following formula was used to describe the relationship between the stagnating average grain radius and particle area fraction and radius:

$$\pi < R >_{\lim}{}^2 \cdot f_V/(\pi r^2) = 3 \tag{15}$$

Figure 8 showed the simulated average number of particles needed to stagnate the grains (ANSPG) for different particle radii and area fractions. As shown in the figure, the ANSPG decreased with the particle radius and not equal to 3. This would lead to the decrease of the total pinning force and the increase of limiting grain size during particle coarsening process. The figure also showed increasing tendencies of the ANSPG with particle area fraction when the particle size was fixed. As the influence of the particle area fraction on the average pinning force per particle was little, the increasing of ANSPG should be the unique reason for the decrease of the limiting grain size when the particle area fraction increased but the particle size was fixed, which corresponding to the precipitation process. Assumed that the relationship between the ANSPG (expressed with $U$ in the equation) and the number of particles per area could still expressed with Equation (15), the following relationships were obtained:

$$\pi < R >_{\lim}^2 \cdot f_V/(\pi r^2) = U \tag{16}$$

where $f_V/(\pi r^2)$ was the number of particles per area. Comparing above equation to Equation (13), the value of $U$ should be written as,

$$U = p f_V{}^q \tag{17}$$

and the following relationships could be obtained:

$$\frac{< R >_{lim}}{r} = \beta_1 \frac{1}{f_V{}^{\xi_1}} \tag{18}$$

$$\beta_1 = \sqrt{p} \tag{19}$$

$$\xi_1 = (1 - q)/2 \tag{20}$$

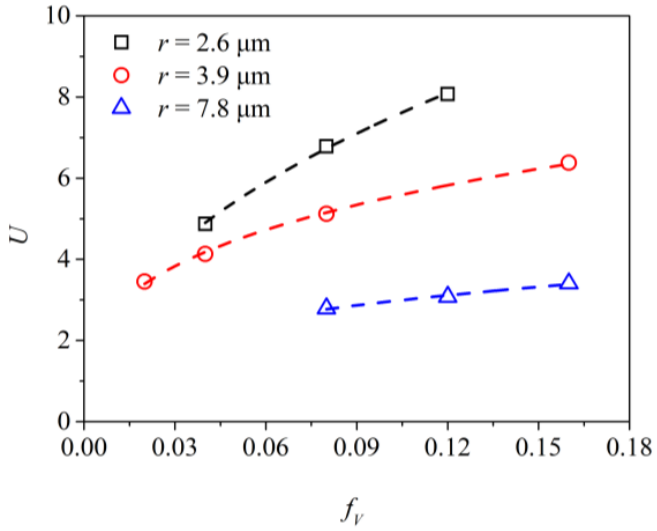



**Figure 8.** Relationships between $U$ and $f_V$ of Equation (17) for different radii.

The parameters $p$ and $q$ in Equation (17) were obtained by non-linear fitting the values in Figure 8. Then the values of $\beta_1$ and $\xi_1$ were calculated with Equations (19) and (20) and shown in Table 2. Table 2 also showed the values of $\beta$ and $\xi$, which were obtained by directly fitting the values of limiting average grain radius, in Equation (13). As shown in Table 2, for small particle radius such as $r$ = 2.6 μm, the values of $\beta_1$ and $\xi_1$ were very close to $\beta$ and $\xi$. However, for large particle radius such as $r$ = 7.8 μm, the value of $\xi$ was larger than $\xi_1$ and the value of $\beta$ was smaller than $\beta_1$. The deviations of the values of $\beta_1$ and $\xi_1$ from $\beta$ and $\xi$ increased with the particle radius. This meant that the relationship between the ANSPG and the number of particles per area deviated from Equation (13), as the particle radius increased. The results indicated that the ANSPG was not only influenced by the number of particles per area, but also influenced by the particle size, which was different to the original assumption of Srolovitz et al. [4]

**Table 2.** The parameters obtained with Equations (13) and (18).

| $r$ (μm) | $\xi$ | $\xi_1$ | $\beta$ | $\beta_1$ |
|---|---|---|---|---|
| 2.6 | 0.26 | 0.26 | 5.3 | 5.2 |
| 3.9 | 0.36 | 0.34 | 3.2 | 3.4 |
| 7.8 | 0.45 | 0.36 | 1.8 | 2.4 |

### *4.4. Comparisons with Other Simulation and Experimental Results*

As proposed in the original research of Hillert [40], pinning force of particles in 2 dimensions was much larger than in 3 dimensions. As the present model was a 2-dimensional cellular model, the simulation results should be compared with 2-dimensional experimental results. However, the interactions between particles and grain boundary in bulk materials were always in 3 dimensions. The thin films should be more similar to the 2-dimensional system. As shown in Figure 9, the simulation results of the present CA model were compared with the results of experiments and other models such as PF and MC models in 2 dimensions. The experimental data were obtained from Al-films containing Θ′-$CuAl_2$ precipitates by Longworth and Thompson [46]. Though the surface grooving of the thin films should influence the grain coarsening kinetics, the 2-dimensional models obtained better simulation results than the 3-dimensional models [21]. In the films, the disc shaped Θ′-$CuAl_2$ precipitates were laid in the columnar grains. Thus, the grain coarsening behavior and the interactions between the grain boundary and particles were 2D. The simulation results of PF and MC models were obtained from the research of Moelans [21] and Gao [8], respectively. In the PF and MC simulations, the radii of the particles were

both given in relative values of lattice site spacing rather than absolute values. To make the results of different models comparable to each other, the ratio of the particle radii to the initial average grain radii, $R_0$, were shown in Figure 9. The values of $r/R_0$ for the experimental results were within 0.1~0.225. As shown in the figure, though the ratio $r/R_0$ of PF and MC models were both close to 0.2, the simulation results of PF model were a little larger than MC model. However, they were both obviously lower than the results of the present model and the experiments. The simulation results for $r/R_0$ = 0.15 and 0.35 for the present models showed better agreement with the experimental results than the PF and MC results. This indicate that the present model could efficiently simulate the grain coarsening processes pinned by the second-phase particles.

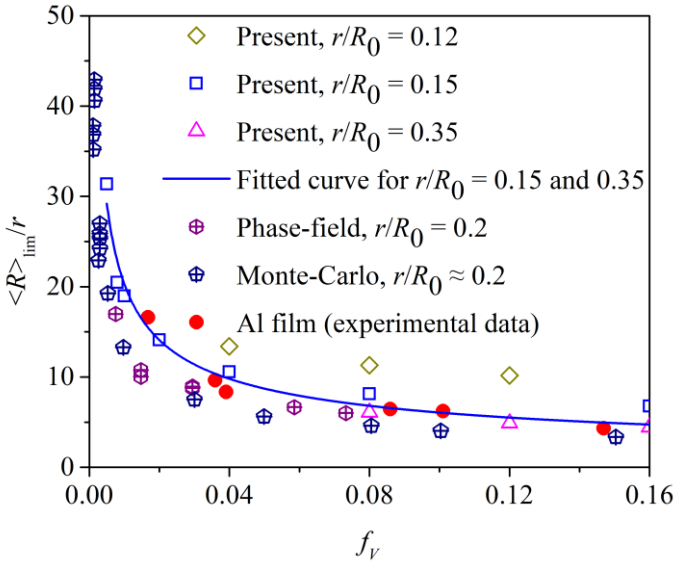



**Figure 9.** The results of the present CA model compared with the PF and MC simulation and experimental results.

## 5. Conclusions

Using a 2D CA model for the particle pinning grain coarsening, the influences of particle changes, such as coarsening, precipitation, growth and dissolution, were investigated by considering the changes of two basic factors: the average pinning force per particle and the particle number density. Then the relationships between the stagnating average grain size and the particle number density were reevaluated. At last, the simulation results of the present model were compared with other simulation and experimental results for validation. The following conclusions were obtained:

(a) The average pinning force per particle was mainly decided by the particle size, but little influenced by the particle number density. This conclusion was different to the traditional theory, which showed the pinning force of a particle was independent of the particle size in 2D. Therefore, the decrease of driving force during the particle coarsening process was the results of the competition between the effects of the size growth and number density decrease of the particles.

(b) The increase of average pinning force per particle with particles size was due to the increase of number fraction of particles in contact with the grain junctions.

(c) The average number of particles for a grain to be stagnated was related to both the number density and size of particles. This was different to the original assumption of Srolovitz et al. [4]

(d) The good agreements between simulation results of the present model and the experimental results showed that the present models were efficient in simulating the second-phase particle pinned grain coarsening processes.

**Author Contributions:** Conceptualization, Z.L. and Y.L.; methodology, Z.L.; software, Y.H.; validation, Z.L., F.P. and S.Z.; formal analysis, S.Z. and Y.H.; investigation, Z.L.; resources, Y.L.; data curation, Z.L.; writing—original draft preparation, Z.L.; writing—review and editing, Y.L. and F.P.; visualization, Z.L. and S.Z.; supervision, Y.L.; project administration, Z.L.; funding acquisition, Z.L. All authors have read and agreed to the published version of the manuscript.

**Funding:** Initial Scientific Research Fund of Young Teachers in Beijing Technology and Business University (QNJJ2021-34).

**Institutional Review Board Statement:** Not applicable.

**Informed Consent Statement:** Not applicable.

**Data Availability Statement:** The datasets generated during and/or analysed during the current study are available from the corresponding author on reasonable request.

**Conflicts of Interest:** The authors declare no conflict of interest.

## References

1. Miura, H.; Tsukawaki, H.; Sakai, T.; Jonas, J. Effect of particle/matrix interfacial character on the high-temperature deformation and recrystallization behavior of Cu with dispersed Fe particles. *Acta Mater.* **2008**, *56*, 4944–4952. [CrossRef]
2. Hutchinson, C.R.; Gouné, M.; Redjaïmia, A. Selecting non-isothermal heat treatment schedules for precipitation hardening systems: An example of coupled process–property optimization. *Acta Mater.* **2007**, *55*, 213–223. [CrossRef]
3. Collins, D.M.; Conduit, B.; Stone, H.; Hardy, M.; Conduit, G.; Mitchell, R. Grain growth behaviour during near-c0 solvus thermal exposures in a polycrystalline nickel-base superalloy. *Acta Mater.* **2013**, *61*, 3378–3391. [CrossRef]
4. Srolovitz, D.J.; Anderson, M.P.; Grest, G.S.; Sahni, P.S. Computer simulation of grain growth-iii. influence of a particle dispersion. *Acta Met.* **1984**, *32*, 1429–1438. [CrossRef]
5. Anderson, M.P.; Grest, G.S.; Doherty, R.D.; Li, K.; Srolovitz, D.J. Inhibition of grain growth by second phase particles: Three dimensional Monte Carlo computer simulations. *Scr. Metall.* **1989**, *23*, 753–758. [CrossRef]
6. Hassold, G.N.; Holm, E.A.; Srolovitz, D.J. Effects of particle size on inhibited grain growth. *Scr. Metall.* **1990**, *24*, 101–106. [CrossRef]
7. Hassold, G.N.; Srolovitz, D.J. Computer simulation of grain growth with mobile particles. *Scr. Metall. et Mater.* **1995**, *32*, 1541–1547. [CrossRef]
8. Gao, J.; Thompson, R.G.; Patterson, B.R. Computer simulation of grain growth with second phase particle pinning. *Acta Mater.* **1997**, *45*, 3653–3658. [CrossRef]
9. Song, X.; Liu, G.; Gu, N. Influence of the second-phase particle size on grain growth based on computer simulation. *Mater. Sci. Eng. A* **1999**, *270*, 178–182. [CrossRef]
10. Miodownik, M.; Holm, E.A.; Hassold, G.N. Highly parallel computer simulations of particle pinning: Zener vindicated. *Scr. Mater.* **2000**, *42*, 1173–1177. [CrossRef]
11. Haghighata, S.M.H.; Taheri, A.K. Investigation of limiting grain size and microstructure homogeneity in the presence of second phase particles using the Monte Carlo method. *J. Mater. Process. Technol.* **2008**, *195*, 195–203.
12. Fjeldberg, E.; Marthinsen, K. A 3D Monte Carlo study of the effect of grain boundary anisotropy and particles on the size distribution of grains after recrystallisation and grain growth. *Comput. Mater. Sci.* **2010**, *48*, 267–281. [CrossRef]
13. Phaneesh, K.; Bhat, A.; Mukherjee, P.; Kashyap, K. On the Zener limit of grain growth through 2D Monte Carlo simulation. *Comput. Mater. Sci.* **2012**, *58*, 188–191. [CrossRef]
14. Riege, S.P.; Thompson, C.V.; Frost, H.J. Simulation of the influence of particles on grain structure evolution in two-dimensional systems and thin films. *Acta Mater.* **1999**, *47*, 1879–1887. [CrossRef]
15. Weygand, D.; Bréchet, Y.; Lépinoux, J. Zener pinning and grain growth: A two-dimensional vertex computer simulation. *Acta Mater.* **1999**, *47*, 961–970. [CrossRef]
16. Weygand, D.; Bréchet, Y.; Lépinoux, J. Inhibition of grain growth by particle distribution: Effect of spatial heterogeneities and of particle strength dispersion. *Mater. Sci. Eng. A* **2000**, *292*, 34–39. [CrossRef]
17. Tamaki, T.; Murakami, K.; Ushioda, K. Proposal of grain growth model based on two-dimensional local curvature multi-vertex model in the presence of pinning particles. *ISIJ Int.* **2016**, *56*, 1857–1865. [CrossRef]
18. Fan, D.; Chen, L.-Q.; Chen, S.-P.P. Numerical simulation of Zener pinning with growing second-phase particles. *J. Am. Ceram. Soc.* **1998**, *81*, 526–532. [CrossRef]
19. Moelans, N.; Blanpain, B.; Wollants, P. A phase field model for the simulation of grain growth in materials containing finely dispersed incoherent second-phase particles. *Acta Mater.* **2005**, *53*, 1771–1781. [CrossRef]
20. Harun, A.; Holm, E.A.; Clode, M.P.; Miodownik, M.A. On computer simulation methods to model Zener pinning. *Acta Mater.* **2006**, *54*, 3261–3273. [CrossRef]
21. Moelans, N.; Blanpain, B.; Wollants, P. Phase field simulations of grain growth in two-dimensional systems containing finely dispersed second-phase particles. *Acta Mater.* **2006**, *54*, 1175–1184. [CrossRef]

22. Chang, K.; Feng, W.; Chen, L.-Q. Effect of second-phase particle morphology on grain growth kinetics. *Acta Mater.* **2009**, *57*, 5229–5236. [CrossRef]
23. Shahandeh, S.; Militzer, M. Grain boundary curvature and grain growth kinetics with particle pinning. *Philos. Mag.* **2013**, *93*, 3231–3247. [CrossRef]
24. Schwarze, C.; Kamachali, R.D.; Steinbach, I. Phase-field study of Zener drag and pinning of cylindrical particles in polycrystalline materials. *Acta Mater.* **2016**, *106*, 59–65. [CrossRef]
25. Chang, K.; Kwon, J.; Rhee, C.-K. Role of second-phase particle morphology on 3D grain growth: A phase-field approach. *Comput. Mater. Sci.* **2016**, *124*, 438–443. [CrossRef]
26. Vedantam, S.; Mallick, A. Phase-field theory of grain growth in the presence of mobile second-phase particles. *Acta Mater.* **2010**, *58*, 272–281.
27. Chang, K.; Chen, L.-Q. Quantitative evaluation of particle pinning force on a grain boundary using the phase-field method, Modelling Simul. *Mater. Sci. Eng.* **2012**, *20*, 05500411.
28. Chang, K.; Kwon, J.; Rhee, C.-K. Effect of particle-matrix coherency on Zener pinning: A phase-field approach. *Comput. Mater. Sci.* **2018**, *142*, 297–302. [CrossRef]
29. Moelans, N.; Blanpain, B.; Wollants, P. Pinning effect of second-phase particles on grain growth in polycrystalline films studied by 3-D phase field simulations. *Acta Mater.* **2007**, *55*, 2173–2182. [CrossRef]
30. Wang, N.; Ji, Y.; Wang, Y.; Wen, Y.; Chen, L.-Q. Two modes of grain boundary pinning by coherent precipitates. *Acta Mater.* **2017**, *135*, 226–232. [CrossRef]
31. Kim, B.N.; Kishi, T. Finite element simulation of Zener pinning behavior. *Acta Mater.* **1999**, *47*, 2293–2301. [CrossRef]
32. Couturier, G.; Maurice, C.; Fortunier, R. Three-dimensional finite-element simulation of Zener pinning dynamics. *Philos. Mag.* **2003**, *83*, 3387–3405. [CrossRef]
33. Li, Z.; Wang, J.; Huang, H. Influences of particle fractions on second-phase particles pinning grain coarsening processes. *J. Mater. Sci.* **2020**, *55*, 3434–3449. [CrossRef]
34. Li, Z.; Wang, J.; Huang, H. Influences of grain/particle interfacial energies on second-phase particle pinning grain coarsening of polycrystalline. *J. Alloys Compd.* **2020**, *818*, 152848. [CrossRef]
35. Turnbull, D. Theory of grain boundary migration rates. *Trans. Met. Soc. AIME* **1951**, *191*, 661–665. [CrossRef]
36. Mason, J.K. Grain boundary energy and curvature in Monte Carlo and cellular automata simulations of grain boundary motion. *Acta Mater.* **2015**, *94*, 162–171. [CrossRef]
37. Li, Z.; Wang, J.; Huang, H. Grain boundary curvature based 2D cellular automata simulation of grain coarsening. *J. Alloys Compd.* **2019**, *791*, 411–422. [CrossRef]
38. Sieradzki, L. Lukasz Made, Comp. *Mater. Sci.* **2013**, *67*, 156–173.
39. Vertyagina, Y.; Mahfouf, M.; Xu, X. 3D modelling of ferrite and austenite grain coarsening using real-valued cellular automata based on transition function. *J. Mater. Sci.* **2013**, *48*, 5517–5527. [CrossRef]
40. Hillert, M. Inhibition of grain growth by second-phase particles. *Acta Metall.* **1988**, *36*, 3177–3181. [CrossRef]
41. Darling, K.; Kapoor, M.; Kotan, H.; Hornbuckle, B.; Walck, S.; Thompson, G.; Tschopp, M.; Kecskes, L. Structure and mechanical properties of Fe-Ni-Zr oxide-dispersion-strengthened ODS alloys. *J. Nucl. Mater.* **2015**, *467*, 205–213. [CrossRef]
42. Barton, D.J.; Kale, C.; Hornbuckle, B.C.; Darling, K.A.; Solanki, K.N.; Thompson, G.B. Microstructure and dynamic strain aging behavior in oxide dispersion strengthened 91Fe-8Ni-1Zr at.% alloy. *Mater. Sci. Eng. A* **2018**, *725*, 503–509. [CrossRef]
43. Kotan, H.; Darling, K.A.; Luckenbaugh, T. High temperature mechanical properties and microstructures of thermally stabilized Fe-based alloys synthesized by mechanical alloying followed by hot extrusion. *Met. Mater. Int.* **2021**, *27*, 1790–1797. [CrossRef]
44. Najafkhani, F.; Kheiri, S.; Pourbahari, B.; Mirzadeh, H. Recent advances in the kinetics of normal/abnormal grain growth: A review. *Arch. Civ. Mech. Eng.* **2021**, *21*, 29. [CrossRef]
45. Smith, C. Zener pinning. *Met. Technol. Trans. Metall. Soc.* **1948**, *1*, 15–51.
46. Longworth, H.P.; Thompson, C.V. Abnormal grain growth in aluminum alloy thin films. *J. Appl. Phys.* **1991**, *69*, 3929–3940. [CrossRef]


**Disclaimer/Publisher's Note:** The statements, opinions and data contained in all publications are solely those of the individual author(s) and contributor(s) and not of MDPI and/or the editor(s). MDPI and/or the editor(s) disclaim responsibility for any injury to people or property resulting from any ideas, methods, instructions or products referred to in the content.